

Fischer, Michael ; Evers, Felix O. ; Formalik, Filip ; Olejniczak, Adam

**Benchmarking DFT-GGA calculations for the structure optimisation of neutral-framework zeotypes**

Journal Article as: peer-reviewed accepted version (Postprint)

DOI of this document\* (secondary publication): <https://doi.org/10.26092/elib/2857>

Publication date of this document: 11/03/2024

\* for better findability or for reliable citation

**Recommended Citation (primary publication/Version of Record) incl. DOI:**

Fischer, M., Evers, F.O., Formalik, F. et al. Benchmarking DFT-GGA calculations for the structure optimisation of neutral-framework zeotypes. *Theor Chem Acc* 135, 257 (2016). <https://doi.org/10.1007/s00214-016-2014-6>

Please note that the version of this document may differ from the final published version (Version of Record/primary publication) in terms of copy-editing, pagination, publication date and DOI. Please cite the version that you actually used. Before citing, you are also advised to check the publisher's website for any subsequent corrections or retractions (see also <https://retractionwatch.com/>).


This version of the article has been accepted for publication, after peer review (when applicable) and is subject to Springer Nature's AM terms of use, but is not the Version of Record and does not reflect post-acceptance improvements, or any corrections. The Version of Record is available online at: <https://doi.org/10.1007/s00214-016-2014-6>

This document is made available with all rights reserved.

**Take down policy**

If you believe that this document or any material on this site infringes copyright, please contact [publizieren@suub.uni-bremen.de](mailto:publizieren@suub.uni-bremen.de) with full details and we will remove access to the material.

# Benchmarking DFT-GGA calculations for the structure optimisation of neutral-framework zeotypes

Michael Fischer<sup>1,2</sup>  · Felix O. Evers<sup>1</sup> · Filip Formalik<sup>3</sup> · Adam Olejniczak<sup>4</sup>

**Abstract** Structure optimisations in the framework of plane-wave density functional theory (DFT) were performed for a set of reference structures of neutral-framework zeotypes and related compounds. The reference set comprised eight all-silica zeolites, four aluminophosphate zeotypes, and two dense polymorphs of SiO<sub>2</sub> ( $\alpha$ -quartz) and AlPO<sub>4</sub> ( $\alpha$ -berlinite). The optimisations considered a total of five GGA-type exchange–correlation functionals (GGA = generalised gradient approximation). Along with the very popular PBE functional, which is well-known to overestimate the lattice dimensions, two GGA functionals designed for solids (WC and PBEsol) and two variants of PBE including a pairwise dispersion correction (PBE-D2 and PBE-TS) were included. A detailed analysis of the agreement between DFT-optimised structures and experimental crystal structure data (obtained for calcined systems) showed that the inclusion of a dispersion correction

greatly improves the prediction of the lattice parameters, with PBE-TS performing particularly well. On the other hand, WC and PBEsol give T–O bond lengths (T = tetrahedral sites) that are in better agreement with experimental data. The accurate reproduction of the T–O–T angles was found to be particularly challenging, as functionals without dispersion correction tend to overestimate these angles, whereas dispersion-corrected variants underestimate them. For all-silica zeolites, the present results were compared to those of a previous DFT study using the hybrid B3LYP-D2 functional and to results of molecular mechanics calculations employing two popular force fields, with none of these methods performing better than PBE-TS or PBE-D2. In order to better understand some of the shortcomings of the functionals considered, additional results for two outliers that were removed from the set of reference structures were analysed. Finally, the ability to reproduce the relative stability was assessed for those SiO<sub>2</sub> frameworks for which experimental enthalpies of transition are available. Here, PBE-D2 outperformed PBE-TS, which showed a systematic tendency to overestimate the energy difference (relative to  $\alpha$ -quartz). On the basis of the present work, PBE-TS can be recommended as a reasonable default choice for structure optimisations of neutral-framework zeotypes. While future benchmarking work could address a wider range of functionals and dispersion correction schemes, it needs to be considered that the limited availability of low-temperature crystal structure data limits the accuracy with which the deviations between computation and experiment can be assessed for this group of materials.

---

**Electronic supplementary material** The online version of this article (doi:[10.1007/s00214-016-2014-6](https://doi.org/10.1007/s00214-016-2014-6)) contains supplementary material, which is available to authorized users.

---

✉ Michael Fischer  
michael.fischer@uni-bremen.de

- <sup>1</sup> Crystallography group, Department of Geosciences, University of Bremen, Klagenfurter Straße, 28359 Bremen, Germany
- <sup>2</sup> MAPEX Center for Materials and Processes, University of Bremen, Bibliotheksstraße 1, 28359 Bremen, Germany
- <sup>3</sup> Group of Bioprocess and Biomedical Engineering, Faculty of Chemistry, Wrocław University of Science and Technology, Wybrzeże Wyspiańskiego 27, 50-370 Wrocław, Poland
- <sup>4</sup> Department of Spectroscopy of Excited States, Institute of Low Temperature and Structure Research, Polish Academy of Sciences, Okólna 2, 50-422 Wrocław, Poland

**Keywords** Zeolites · Density functional theory · Dispersion correction · Benchmarking · Solid state chemistry

## 1 Introduction

Zeolites are porous crystalline materials that play a “cornerstone” role in various applications, such as catalysis, adsorption-based separations, and ion exchange (water softening) [1]. As a complement to experimental characterisation techniques, computational investigations have greatly contributed to an atomic-level understanding of these materials. A recent review by Van Speybroeck et al. [2] provides a comprehensive overview of the applications of computational chemistry techniques in zeolite science, covering both molecular mechanics and electronic structure calculations. In the latter field, density functional theory (DFT) plays a particularly prominent role, as it combines a high achievable accuracy with a moderate computational cost. On the one hand, the efficiency of DFT permits comparative studies of a large number of zeolite structures, exemplified by the DFT-based prediction of the elastic properties of 121 zeolite frameworks by Coudert [3]. On the other hand, the treatment of structures with very large unit cells is also possible. In previous work, we used DFT calculations to calculate system-specific charges for a variety of zeolites, the largest unit cell having a volume of more than 20,000 Å<sup>3</sup> (primitive cell of PAU framework) [4].

It is well established that the result of a DFT calculation—and, thus, its potential usefulness—depends strongly on the choice of the exchange–correlation functional. As a consequence, the “benchmarking” of DFT calculations, i.e. the critical comparison of different functionals, has become a very active field of research. In such benchmarking studies, either experimental data or computational results from high-level wave-function-based methods (e.g. coupled-cluster calculations) are used as reference data. Depending on the quantity one aims to predict, most emphasis in the benchmarking can be placed on the accurate prediction of structures, energetics (thermochemistry), or other properties (e.g. vibrational spectra). An additional problem arises when dispersion interactions play a non-negligible role in the system of interest, as these interactions are not well represented in DFT calculations employing standard exchange–correlation functionals (such as the local density approximation (LDA), the generalised gradient approximation (GGA), or hybrid functionals) [5, 6]. To address this issue, different approaches of varying complexity have been proposed to incorporate dispersion interactions in DFT [5–8], leading to an additional degree of freedom in the setup of the computations. Benchmarking efforts in the field of organic non-covalent complexes, for which the accurate description of both intra- and intermolecular interactions is pivotal, have been presented, for example, by Grimme et al. [9, 10]. Other groups have focussed on the structure prediction of molecular crystals, where crystal packing effects play an important role [11–13]. To

emphasise the wide variety of possibilities, it is worth noting that a single benchmarking study on small non-covalent dimers included a total of 382 different “flavours” of DFT (different exchange–correlation functionals with and without dispersion correction) [14].

Numerous researchers have investigated the performance of DFT for the prediction of structures and properties of inorganic crystalline solids. It has been established that LDA, the simplest approximation, tends to “overbind” structures, causing an underestimation of bond lengths and lattice parameters, whereas the opposite trend is observed for many GGA-type functionals (e.g. the PBE functional [15], which is particularly popular for solids) [16, 17]. While a complete discussion of previous DFT benchmarking efforts for inorganic crystals is beyond the scope of the present work, some results of particular relevance are summarised in the following. In order to discuss some of the most typical observations, the very recent study of Tran et al. [18] provides a good starting point. These authors compared the performance of a large portfolio of DFT approaches, comprising LDA, GGA, meta-GGA, and hybrid functionals, both with and without dispersion corrections, for lattice constants, bulk moduli, and cohesive energies of strongly bound and dispersion-dominated solids. For the strongly bound solids (elements and binary compounds, a total of 44 systems), some GGA-type functionals that were specifically designed for solids (such as the Wu-Cohen [WC] [19], PBEsol [20], and SG4 [21] functionals) provided results that were similarly accurate to those obtained with the best-performing meta-GGA and hybrid functionals. While the use of a dispersion correction did not always lead to better results, the authors observed a significant improvement in cases where the uncorrected functional had a clear tendency to overestimate the lattice parameters, e.g. for PBE. For systems in which dispersion interactions are important (rare gas crystals and layered solids, a total of 5 systems), none of the uncorrected functionals gave a satisfactory performance across the board, while the inclusion of a pairwise (Grimme-type) [22, 23] dispersion correction improved the results considerably.

A good performance of PBEsol and WC for the prediction of equilibrium structures was also observed in a series of comparative studies of different minerals ( $\alpha$ -quartz, corundum, forsterite, pyrope, Al<sub>2</sub>SiO<sub>5</sub> polymorphs) [24–26]. However, these functionals failed in the description of hydrogen-bonded layered aluminium hydroxides, where the length of hydrogen bonds was severely underestimated, and also for the case of brucite, Mg[OH]<sub>6</sub>, in which the layers are held together by dispersion interactions. For these systems, hybrid functionals, which incorporate a fraction of exact (Hartree–Fock) exchange and are thus computationally more demanding, were found to give better agreement with experiment [26]. A superior performance of

these functionals was also found in a computational study of anhydrous and hydrated clinoptilolite, a natural zeolite [27]. Moreover, hybrids are better suited than GGA-type functionals when aiming at the computation of vibrational spectra [24–26] or band gaps [28].

In order to understand whether the accuracy can be improved by including a dispersion correction term, Tunega et al. [29] compared the performance of different GGA-type functionals (among them PBE and PBEsol), including some dispersion-corrected variants, in the prediction of the structural parameters of four clay minerals, where the layers are held together either by dispersion forces (talca, pyrophyllite) or by hydrogen bonds (lizardite, kaolinite). At variance with the previously discussed results on layered aluminium hydroxides and brucite, these authors observed a good performance of the PBEsol functional (without dispersion correction) for all four systems. Among the dispersion-corrected approaches, the PBE-TS functional [30] gave particularly good agreement with the experimental structures, while a moderate, but systematic, underestimation of the lattice parameters was found for PBE with the Grimme-type D2 correction [22]. Using hybrid functionals (PBE0 [31], B3LYP [32, 33]), Román-Román and Zicovich-Wilson [34] showed that the prediction of the relative stability of all-silica zeolites is improved by the inclusion of a dispersion correction. Interestingly, these authors observed a systematic overestimation of the molar volume (volume per  $\text{SiO}_2$  unit), which may exceed 10% for some zeolites even for the best-performing approach (PBE0-D2).

The large majority of previous studies of zeolites that compared the performance of different DFT approaches typically addressed only one or a few systems (e.g. an extensive benchmarking work addressing structure and various properties of Co- and Cu-exchanged chabazite [35–37], the previously mentioned study of clinoptilolite [27], and a very recent investigation of MFI nanosheets [38]) and/or focussed on the interaction of zeolite hosts with adsorbed molecules (e.g. water [39–41], NO [42], CO [43–45],  $\text{CO}_2$ ,  $\text{CH}_4$  and  $\text{N}_2$  [46], alkanes and/or alcohols [47–53]). While the study of Román-Román and Zicovich-Wilson [34] covers a total of 14 all-silica zeolites, these authors only reported the molar volumes, without discussing the structural parameters in more detail. In contrast, a benchmarking of DFT approaches that places most emphasis on the accurate reproduction of guest-free zeolite structures, considering a range of different topologies, has not yet been carried out. In order to fill this gap, the present study evaluates the performance of GGA-type functionals based on PBE in the crystal structure optimisation of neutral-framework zeotypes, more specifically, all-silica ( $\text{SiO}_2$ ) zeolites and aluminophosphate ( $\text{AlPO}_4$ ) zeotypes. As these materials do not contain any extra-framework cations (for which fractional occupancies are the rule, rather than the

exception), and no mixed occupancies of the tetrahedral sites (which also occur very frequently in aluminosilicate zeolites), there is no necessity to modify the experimental structures in order to arrive at models that can be used in the DFT computations. Because the DFT-optimised structures are directly comparable to experimental crystal structure data, these neutral-framework zeotypes are particularly well suited for benchmarking purposes.

In addition to the original PBE functional and two PBE-based functionals that were specifically designed for solids (WC, PBEsol), two dispersion-corrected variants (PBE-D2 and PBE-TS) are included. As outlined above, WC and PBEsol perform well for dense solids, but less so for layered systems due to the poor description of the inter-layer interactions, where dispersion-corrected functionals are more accurate. Taken together, these findings do not provide clear guidelines for zeolites and related materials: while the three-dimensional connectedness of the framework indicates that WC/PBEsol should perform rather well for these systems, long-range interactions across the pores might also play a non-negligible role in determining the equilibrium structure, necessitating the inclusion of a dispersion correction term. The present selection of functionals allows us order to determine the relative importance of an accurate description of “short-range” and “long-range” effects. Although rather poor agreement with experiment can be expected for standard PBE, it is included as a reference functional to evaluate the relative improvement by using “post-PBE” approaches.

While it might be argued that a larger range of functionals should be included in the benchmarking, it should be reiterated that some of the functionals considered have been found to perform very well for related materials, such as sheet silicates [29]. Moreover, GGA-type functionals are particularly attractive due to their modest computational cost and may thus be employed for tasks where the use of more sophisticated functionals (meta-GGA, hybrids) is not (yet) feasible. To this end, the present study aims to elucidate how accurate results one can obtain with a relatively low-level DFT approach. Future work could then address whether the use of more elaborate functionals enables further improvements.

The remainder of this paper is organised as follows: after describing the choice of reference structures, the computational methods, and the means of error assessment, the results and discussion section begins with a detailed analysis of the DFT-optimised structures in terms of the errors in lattice parameters, T–O bond distances, and T–O–T bond angles (T represents the tetrahedral sites, i.e. the positions occupied by silicon, aluminium, or phosphorus). The resulting errors are then compared to previous calculations using a dispersion-corrected hybrid functional (B3LYP-D2) from the literature [3] and to molecular mechanics calculations

employing two different force fields. Furthermore, results for two “outliers” that were removed from the set of reference structures are presented and analysed. Finally, it is assessed how the GGA-type functionals perform in the prediction of the relative stabilities of porous SiO<sub>2</sub> polymorphs relative to  $\alpha$ -quartz.

## 2 Materials and methods

### 2.1 Choice of reference structures

In order to choose a suitable set of all-silica and aluminophosphate zeotypes, only systems fulfilling the following criteria were selected:

1. The material has (nearly) perfect SiO<sub>2</sub> or AlPO<sub>4</sub> composition, and there are no signs of structural disorder.
2. The experimental structure determination was performed for the calcined material, without structure-directing agents or solvent molecules in the pores.
3. The experimentally determined structure was obtained at room temperature or lower temperatures.
4. The T–O distances in the structures are not too far away from the expected equilibrium distance. For example, the Si–O distances in the all-silica zeolites considered fall between  $\sim 1.57$  and  $1.64$  Å. A somewhat larger tolerance was allowed for Al–O and P–O distances in AIPOs. Similarly, systems were ruled out if peculiar deviations of the O–T–O angles from the ideal tetrahedral angle occur (such deviations were observed, for example, in the all-silica zeolite GUS-1 [GON topology], which contains O–T–O angles of  $\sim 95^\circ$  and  $\sim 127^\circ$  [54]).
5. There are no T–O–T angles of  $180^\circ$  in the structure, since these are considered to be the result of disorder around a high-symmetry position. In one prominent example, early determinations of the ferrierite (FER) structure in space group *Immm* included one linearly coordinated oxygen atom, for which the angle is fixed to  $180^\circ$  due to the site symmetry [55–57]. It was later shown that a refinement in a space group with lower symmetry results in an angle of  $\sim 170^\circ$  [29] around this oxygen atom [58, 59].
6. Finally, the unit cell should not exceed a certain size to render the DFT calculations feasible. Computations for all-silica faujasite (FAU framework), which has a large unit cell with an edge length of  $\sim 25$  Å, were performed by using the primitive cell in the DFT calculations. The structure was transformed back to the conventional (face-centred) cell for the comparison with experiment. In all other cases, the conventional cell was used.

Based on these criteria, suitable zeotypes were identified by making use of the ZeoBase database [60] as well as the IZA structure database [61]. The final set of reference structures consisted of eight all-silica zeolites and four aluminophosphates. Additionally, two dense polymorphs of SiO<sub>2</sub> and AlPO<sub>4</sub>,  $\alpha$ -quartz and  $\alpha$ -berlinite, were included. Further calculations were performed for two other zeotypes, all-silica SOD (sodalite) and all-silica AST. However, an analysis of the error in lattice parameters revealed unusually large deviations (in comparison to all other systems), leading to a very large impact of these systems on the overall error. These two zeotypes were thus omitted from the overall error analysis. In order to develop some possible explanations why the chosen DFT approaches perform less satisfactorily in these cases, the results for SOD and AST are discussed separately towards the end of the article.

Table 1 gives an overview of all systems considered in this study, with references to the articles in which the experimental structure data were published. In the large majority of cases, the experimental diffraction measurements used for the structure determination were performed at room temperature, the three exceptions being ITQ-4 (IFR framework,  $T_{\text{meas}} = 30$  K), ZSM-22 (TON framework,  $T_{\text{meas}} = 120$  K), and AIPO-34 (CHA framework,  $T_{\text{meas}} = 110$  K). It is worth noting that the selection of zeotypes is not limited to a certain window size, but contains systems with accessible pores linked by 8-, 10-, or 12-ring windows (and combinations thereof). The structures are visualised in Fig. 1.

### 2.2 Computational details

All DFT calculations were carried out with the CASTEP code (version 7.01), which uses a combination of plane waves and pseudopotentials [62]. “Core” electrons were represented using on-the-fly-generated ultrasoft pseudopotentials, and an energy cut-off of 800 eV was employed, which was found to give very well-converged total energies (the finite basis correction term  $\delta E_{\text{tot}}/\delta \log(E_{\text{cut}})$  was well below 0.01 eV per atom for all systems, indicating very good convergence [63]). For each system, calculations using different numbers of  $k$ -points were performed to ensure convergence with respect to the size of the  $k$ -point mesh. The  $k$ -point meshes that were found to give converged results are included in Table 1.

As mentioned above, the following exchange–correlation functionals were considered:

- The very popular PBE functional [15], whose deficiencies in predicting lattice parameters have been well documented [16, 17].



**Table 1** Overview of systems included in this study

Framework type	Composition	Name/acronym	Space group (ITA No.)	Rings	$k$ -mesh	References
qtz	SiO <sub>2</sub>	$\alpha$ -Quartz	$P3_221$ (154)	–	$4 \times 4 \times 4$	[64]
qtz	AlPO <sub>4</sub>	$\alpha$ -Berlinite	$P3_121$ (152)	–	$4 \times 4 \times 2$	[65]
CHA	SiO <sub>2</sub>	–	$R\bar{3}m$ (166)	8, 6, 4	$1 \times 1 \times 1$	[66]
FAU	SiO <sub>2</sub>	ZDDAY <sup>a</sup>	$Fd\bar{3}m$ (227)	12, 6, 4	$1 \times 1 \times 1$	[67]
FER	SiO <sub>2</sub>	–	$Pm\bar{m}n$ (58)	10, 8, 6, 5	$1 \times 1 \times 2$	[59]
IFR	SiO <sub>2</sub>	ITQ-4	$I2/m^b$ (12)	12, 6, 5, 4	$1 \times 1 \times 2$	[68]
LTA	SiO <sub>2</sub>	ITQ-29	$Pm\bar{3}m$ (221)	8, 6, 4	$2 \times 2 \times 2$	[69]
RTE	SiO <sub>2</sub>	RUB-3	$C2/m$ (12)	8, 6, 5, 4	$1 \times 1 \times 2$	[70]
SAS	SiO <sub>2</sub>	SSZ-73	$I4/mmm$ (139)	8, 6, 4	$1 \times 1 \times 1$	[71]
TON	SiO <sub>2</sub>	ZSM-22	$Cmc2_1$ (36)	10, 6, 5	$2 \times 1 \times 3$	[72]
AEN	AlPO <sub>4</sub>	AIPO-53(B)	$Pbca$ (61)	8, 6, 4	$1 \times 1 \times 1$	[73]
CHA	AlPO <sub>4</sub>	AIPO-34	$R\bar{3}$ (148)	8, 6, 4	$1 \times 1 \times 1$	[74]
ERI	AlPO <sub>4</sub>	AIPO-17	$P6_3/m$ (176)	8, 6, 4	$1 \times 1 \times 1$	[75]
EZT	AlPO <sub>4</sub>	EMM-3	$I2/m^b$ (12)	12, 8, 6, 4	$2 \times 2 \times 1$	[76]
AST	SiO <sub>2</sub>	Octadecasil	$I4/m$ (87)	6, 4	$2 \times 2 \times 2$	[77]
SOD	SiO <sub>2</sub>	–	$R\bar{3}$ (148)	6, 4	$1 \times 1 \times 2$	[78]

In addition to framework type code, acronym or mineral name, and space group, the kinds of N-membered rings that are present in the structure are given for all zeotypes [61]. The  $k$ -point mesh used in the DFT calculations is also included

<sup>a</sup> ZDDAY stands for “zero-defect dealuminated zeolite Y”

<sup>b</sup> Non-standard setting of  $C2/m$

- Two functionals that are based on PBE, but aim at an improved prediction of the structure and properties of solids: WC [19] and PBEsol [20].
- The PBE functional combined with two different pairwise dispersion correction schemes: while the PBE-D2 approach devised by Grimme uses one fixed set of dispersion coefficients [22], the PBE-TS approach proposed by Tkatchenko and Scheffler scales the dispersion coefficients on the basis of a Hirshfeld partitioning of the DFT electron density [30].

In all cases, the lattice parameters and all atomic coordinates (unless constrained by symmetry) were relaxed in the structure optimisations. Calculations were considered converged when the following criteria were fulfilled simultaneously: Forces on all atoms are below  $10^{-3}$  eV  $\text{\AA}^{-1}$ , maximal atomic displacement from one optimisation step to the next is less than  $5 \times 10^{-4}$   $\text{\AA}$ , the energy change from one step to the next is below  $10^{-6}$  eV, and residual stress is below  $5 \times 10^{-3}$  GPa. CIF files of all optimised structures (generated by CASTEP through the `write_cif_structure` flag), as well as one representative CASTEP parameter (.param) and structure (.cell) file are supplied as Electronic Supplementary Material.

### 2.3 Assessment of errors

For any individual structural parameter  $x$ , the absolute deviation between DFT calculation and experiment was calculated as:

$$err_x = x_{\text{DFT}} - x_{\text{exp}}$$

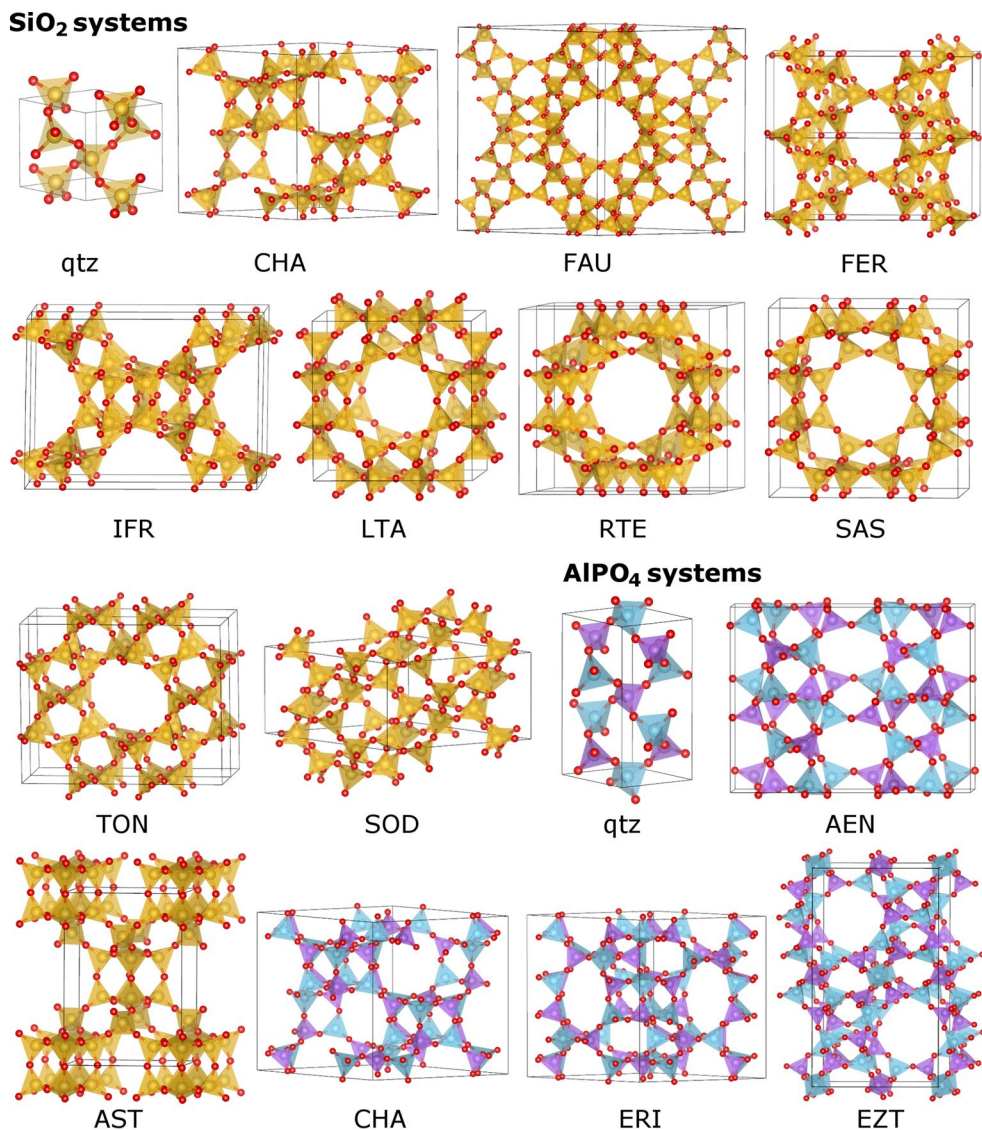
The following structural parameters were considered in the analysis: the lattice parameters  $a$ ,  $b$ ,  $c$ , the T–O bond lengths, and the T–O–T angles. Every non-equivalent parameter was counted once in the sums given below, which means that a cubic system contributes only one error value to the calculated overall errors in lattice parameters, whereas an orthorhombic system contributes three. Similarly, bond lengths and angles were not weighted according to the multiplicity. As there are three monoclinic systems among the structures considered, it would in principle also be necessary to include the monoclinic angle in the error analysis. However, it was found that deviations in this angle from the experimental value are always small, regardless of the choice of functional, remaining below  $0.5^\circ$  ( $\sim 0.5\%$ ), which is why the angle was omitted from the further analysis.

In order to evaluate the overall error, both the mean of absolute errors and the mean of signed errors were calculated. The mean of signed errors ( $MSE$ ) is calculated as [28]:

$$MSE = \frac{1}{N_i} \sum_{i=1}^{N_i} err_{x,i}$$

The mean of absolute errors ( $MAE$ ), also referred to as mean absolute deviation, corresponds to [28]:

**Fig. 1** Visualisation of all  $\text{SiO}_2$  and  $\text{AlPO}_4$  frameworks considered. Structure drawings were prepared with VESTA [79]



$$MAE = \frac{1}{N_i} \sum_{i=1}^{N_i} |err_{x,i}|$$

While the T–O bond lengths and T–O–T angles all fall reasonably close to an average value, the lattice parameters span a range from 5 to 25 Å. This renders it useful to also consider relative deviations, which were evaluated using the root mean square of relative errors (*RMSE*):

$$RMSE = \sqrt{\frac{1}{N_i} \sum_{i=1}^{N_i} \left( 100 \cdot \frac{err_{x,i}}{x_{exp,i}} \right)^2}$$

Finally, the largest individual errors (in absolute and, where useful, relative terms) were also evaluated. The errors obtained for the individual systems are compiled in a Microsoft EXCEL file, which is part of the Electronic Supplementary Material.

It is obvious that the accuracy of the experimental data will determine the outcome of the error analysis. As there are no means to evaluate this accuracy on the basis of literature data, it is assumed that the errors in the experimental structure determinations are much smaller than the deviations between DFT and experiment. Nevertheless, two aspects of particular importance should be highlighted in this context:

1. The DFT-optimised structures correspond to the equilibrium structures at 0 K, whereas the experimental structures were determined from datasets measured at room temperature (or, in some instances, lower temperatures, see above). Therefore, a certain difference in the lattice parameters has to be expected due to (positive/negative) thermal expansion of the real system, which is not accounted for in the calculations. The thermal expansion of several of the systems considered in the present work

**Table 2** Overall errors in lattice parameters in absolute and relative terms (*MSE*, *MAE*, *RMSE*), as well as largest signed error (*LSE*) and largest relative error (*LRE*) found among the individual results

SiO <sub>2</sub> systems	PBE	WC	PBEsol	PBE-D2	PBE-TS
<i>MSE</i> /Å	+0.145	+0.084	+0.074	+0.056	+0.044
<i>MAE</i> /Å	0.145	0.086	0.076	0.058	0.047
<i>RMSE</i> /%	1.37	0.87	0.71	0.52	0.44
<i>LSE</i> /Å	+0.280 ( <i>b</i> , TON)	+0.211 ( <i>b</i> , TON)	+0.172 ( <i>b</i> , TON)	+0.142 ( <i>a</i> , FAU)	+0.113 ( <i>a</i> , FAU)
<i>LRE</i> /%	+2.34 ( <i>a</i> , α-quartz)	+1.86 ( <i>c</i> , TON)	+1.39 ( <i>c</i> , TON)	+1.12 ( <i>c</i> , SAS)	+0.86 ( <i>c</i> , SAS)
AlPO <sub>4</sub> systems					
<i>MSE</i> /Å	+0.153	+0.080	+0.071	+0.052	+0.034
<i>MAE</i> /Å	0.153	0.080	0.071	0.079	0.060
<i>RMSE</i> /%	1.36	0.79	0.65	0.66	0.52
<i>LSE</i> /Å	+0.239 ( <i>c</i> , ERI)	+0.183 ( <i>c</i> , ERI)	+0.157 ( <i>c</i> , ERI)	+0.265 ( <i>a</i> , AEN)	+0.169 ( <i>a</i> , AEN)
<i>LRE</i> /%	+2.39 ( <i>a</i> , α-berlinite)	+1.38 ( <i>a</i> , α-berlinite)	+1.07 ( <i>b</i> , EZT)	+1.47 ( <i>a</i> , AEN)	+1.09 ( <i>a</i> , ERI)

has been studied experimentally, e.g. for α-quartz [64], ITQ-4 (IFR) [68], and AIPO-34 (CHA) [74]. An estimation based on the thermal expansion coefficients determined in those works indicates that the relative difference in lattice parameters between room temperature and 0 K is usually smaller than 0.5%. As we will see below, the deviations between DFT and experiment are typically larger, and it can thus be expected that the neglect of thermal expansion does not affect the overall conclusions.

- It has been pointed out that the “apparent” Si–O bond lengths that are obtained from X-ray diffraction measurements at room temperature are shorter than the actual bond lengths due to correlated motion of the SiO<sub>4</sub> tetrahedra [80]. A correction for these (translational, librational, and screw) effects leads to an increase in the bond length of approximately 0.005 Å with respect to the “apparent” Si–O bond length at room temperature (this correction is even more pronounced for higher temperatures). While this effect has, to our knowledge, not yet been analysed in detail for aluminophosphates, a similar magnitude can be expected on the grounds of the similar bonding situation.

Throughout this study, all comparisons will be made with lattice parameters, bond lengths, and bond angles that were directly taken from experiment, i.e. without applying any corrections. Where appropriate, however, the discussion will take the aforementioned points into account.

### 3 Results and discussion

#### 3.1 Error analysis I: lattice parameters

Table 2 reports the errors in the lattice parameters obtained for the DFT-optimised structures, giving separate results

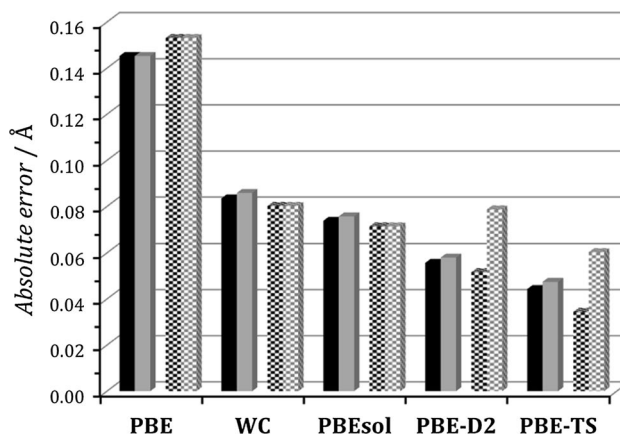


**Fig. 2** *MSE* and *MAE* in lattice parameters. For each functional, the bars from left to right represent: *MSE* (black, filled) and *MAE* (grey, filled) for SiO<sub>2</sub> systems, *MSE* (black, checkered) and *MAE* (grey, checkered) for AlPO<sub>4</sub> systems

for SiO<sub>2</sub> systems (α-quartz and eight all-silica zeolites) and AlPO<sub>4</sub> systems (α-berlinite and four aluminophosphate zeotypes). Furthermore, the mean of signed errors and mean of absolute errors are visualised in Fig. 2. Looking at the overall errors found for the SiO<sub>2</sub> systems, it is apparent that, for the PBE, WC, and PBEsol functionals, *MSE* and *MAE* are practically equal, i.e. (virtually) all lattice parameters are overestimated. The overall error is reduced from approximately 0.15 Å to slightly below 0.1 Å when moving from PBE to either of the GGA functionals for solids, with PBEsol performing somewhat better than WC. The smallest errors in the range of 0.05 Å are observed for the two dispersion-corrected approaches, PBE-D2 and PBE-TS. Even for these functionals, the values of *MSE* and *MAE* remain fairly similar, since the lattice parameters are still overestimated for most systems (an underestimation is found for four/three of 20 individual lattice parameters for PBE-D2/



**Table 3** Average Si–O, Al–O, and P–O bond distances and overall errors in absolute terms (*MSE*, *MAE*) and largest signed errors (*LSE*) found among the individual results

	Exp	PBE	WC	PBEsol	PBE-D2	PBE-TS
Si–O bonds						
$d_{\text{aver}}/\text{\AA}$	1.601	1.615	1.608	1.609	1.615	1.614
$MSE/\text{\AA}$	–	+0.014	+0.007	+0.008	+0.014	+0.013
$MAE/\text{\AA}$	–	0.015	0.010	0.010	0.015	0.014
$LSE/\text{\AA}$	–	+0.038	+0.031	+0.032	+0.039	+0.038
Al–O bonds						
$d_{\text{aver}}/\text{\AA}$	1.722	1.741	1.732	1.733	1.738	1.737
$MSE/\text{\AA}$	–	+0.019	+0.011	+0.011	+0.016	+0.015
$MAE/\text{\AA}$	–	0.024	0.021	0.021	0.023	0.022
$LSE/\text{\AA}$	–	+0.082	+0.074	+0.074	+0.083	+0.082
P–O bonds						
$d_{\text{aver}}/\text{\AA}$	1.528	1.529	1.522	1.523	1.529	1.528
$MSE/\text{\AA}$	–	+0.001	–0.006	–0.005	+0.001	–0.000
$MAE/\text{\AA}$	–	0.017	0.017	0.017	0.017	0.016
$LSE/\text{\AA}$	–	–0.050	–0.058	–0.058	–0.055	–0.056

PBE-TS). In accordance with the observations made for the absolute errors, the smallest relative error (*RMSE*) is found for the PBE-TS functional, closely followed by PBE-D2. Regarding the largest individual errors, the values of *LSE* and *LRE* obtained for the best-performing functional, PBE-TS, amount to +0.11 Å and +0.9%, respectively, whereas the corresponding values for PBE are more than twice as large. In other words, the PBE-TS functional predicts all lattice parameters of the nine SiO<sub>2</sub> systems with an error of less than 1%, a rather impressive performance.

For the compounds with aluminophosphate composition, very similar trends in *MSE*, *MAE*, and *RMSE* as for the SiO<sub>2</sub> systems are found. However, an increased *MAE* and fairly large values of *LSE/LRE* are observed for the dispersion-corrected functionals. A closer look at the individual lattice parameters shows that this is primarily due to the results for AEN, where PBE-D2 and, to a lesser extent, PBE-TS overestimate the length of the *a*-axis, but underestimate the length of the *b*-axis. An inspection of the optimised structures reveals rather large deviations from the experimental structure in the dimensions of the eight-ring windows of AEN, which are elliptically distorted. As a similar behaviour is observed for the “outliers”, all-silica SOD and AST, the apparent problems of dispersion-corrected functionals in dealing with systems having distorted windows will be discussed in more detail below.

As a final remark to this section, it has to be reiterated that the differences between the lattice parameters obtained at room temperature and their equilibrium values at 0 K are likely to amount to a few tenths of a per cent. A more accurate error assessment for the different functionals would need to account for this effect; however, the lack of available low-temperature data precludes a quantitative analysis.

From a qualitative perspective, it is worth noting that many systems, among them CHA-SiO<sub>2</sub>, AIPO-34 (CHA), and ITQ-4 (IFR), exhibit negative thermal expansion (NTE) [68, 74, 81, 82]. As the DFT calculations typically deliver larger lattice parameters than experiment, the agreement should improve further if NTE was accounted for.

### 3.2 Error analysis II: T–O bond lengths and T–O–T angles

The average Si–O, Al–O, and P–O bond lengths, as well as the values of *MSE*, *MAE*, and *LSE*, for all five functionals are compiled in Table 3. In Fig. 3, the distribution of the bond lengths in the experimental structures is compared to the analogous distributions in the structures optimised with the PBE, PBEsol, and PBE-TS functionals (results for WC and PBE-D2 are omitted from the figure because they are very similar to those obtained with PBEsol and PBE-TS, respectively). The overall errors obtained with these three functionals are visualised in Fig. 4.

It is worth noting that PBE, PBE-D2, and PBE-TS give practically identical bond lengths. This behaviour is not unexpected, since the dispersion correction should have no significant impact on the representation of interactions between atoms that are directly bonded to each other. It is also apparent that PBEsol and WC predict bond lengths that are systematically shorter than PBE and its dispersion-corrected variants, the typical difference amounting to ~0.007 Å. Furthermore, it is worth noting that the DFT calculations always lead to a much narrower distribution of the distances when compared to experiment. For example, the difference between the shortest and longest Si–O bond in the experimental structures amounts to ~0.07 Å, whereas

**Fig. 3** Distribution of T–O bond lengths among all zeolite types considered. *Left* Si–O bond lengths in all-silica zeolites. *Right* Al–O bond lengths (black) and P–O bond lengths (grey) in aluminophosphates. Results for the WC and PBE-D2 functionals are omitted due to their similarity to PBEsol and PBE-TS results, respectively

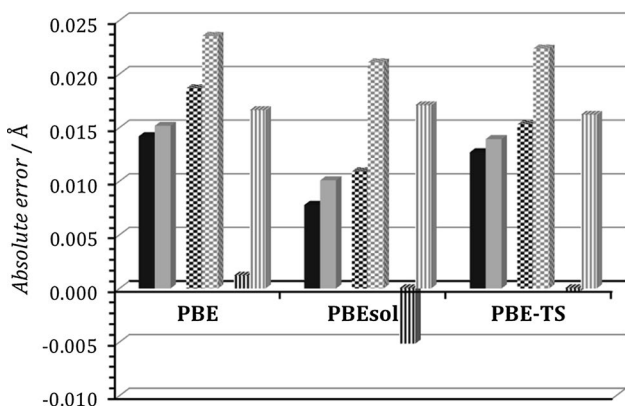
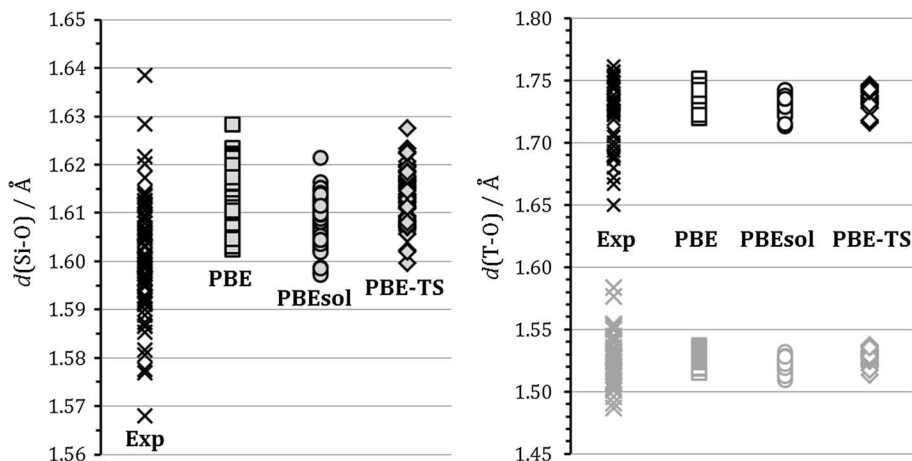


**Fig. 4** *MSE* and *MAE* in T–O bond lengths for PBE, PBEsol, and PBE-TS functionals. For each functional, the bars represent (from left to right): *MSE* (black, filled) and *MAE* (grey, filled) for Si–O bonds, *MSE* (black, checkered) and *MAE* (grey, checkered) for Al–O bonds, *MSE* (black, striped) and *MAE* (grey, striped) for P–O bonds

all DFT-optimised Si–O bond lengths fall within 0.03 Å. This trend is even more pronounced for Al–O and P–O bonds. This is not a surprising finding, as the DFT calculations will always optimise the bonds until they are close to their equilibrium value, because any appreciable deviation from the equilibrium distance will incur an energetic “penalty”. Therefore, unusually short or long bonds observed in the experimental structures will become longer or shorter during the DFT optimisation. Similar observations were made in our previous work on H<sub>2</sub>O-containing zeolites, where the DFT calculations led to a narrowing of the distribution of O<sub>water</sub>–H<sub>water</sub> distances when compared to experiment [41].

A quantitative comparison of the DFT-optimised Si–O distances to experimental values shows that the bond lengths predicted by PBE/PBE-D2/PBE-TS are, on average, approximately 0.015 Å too long, while WC and PBEsol overestimate the bond lengths by roughly 0.01 Å

(as discussed previously, the similar magnitude of *MSE* and *MAE* corresponds to systematic overestimation). For Al–O bonds, increased values of *MSE* and *MAE* are found for all functionals, and there is also a systematic tendency to overestimate the bond length. A different behaviour is observed for the P–O bonds: While the average deviation between DFT and experiment, reflected in the *MAE*, falls between those observed for Si–O and Al–O bonds, the *MSE* is much closer to zero, indicating no tendency towards a systematic over- or underestimation. In particular, the WC and PBEsol functionals tend to deliver slightly shorter P–O bonds than experiment.

In line with the aforementioned tendency of DFT to optimise the bond distances towards their equilibrium values, the largest errors are always observed for bonds that are either unusually short (e.g. Si1–O2 in LTA:  $d_{\text{exp}} = 1.568$  Å, Si1–O1 in RTE:  $d_{\text{exp}} = 1.577$  Å, Al1–O2 in AEN:  $d_{\text{exp}} = 1.650$  Å) or unusually long (Al3–O1 bond in AEN:  $d_{\text{exp}} = 1.748$  Å) in the experimental structures. As a consequence of the tendency of DFT to give slightly longer Si–O and Al–O bond lengths than experiment, the largest errors always occur in cases where the bond length is overestimated. The opposite is found for P–O bonds: here, the most prominent deviations are found for the P2–O11 and P1–O3 bonds in AEN, which are very long in the experimental structure ( $d_{\text{exp}} \approx 1.58$  Å).

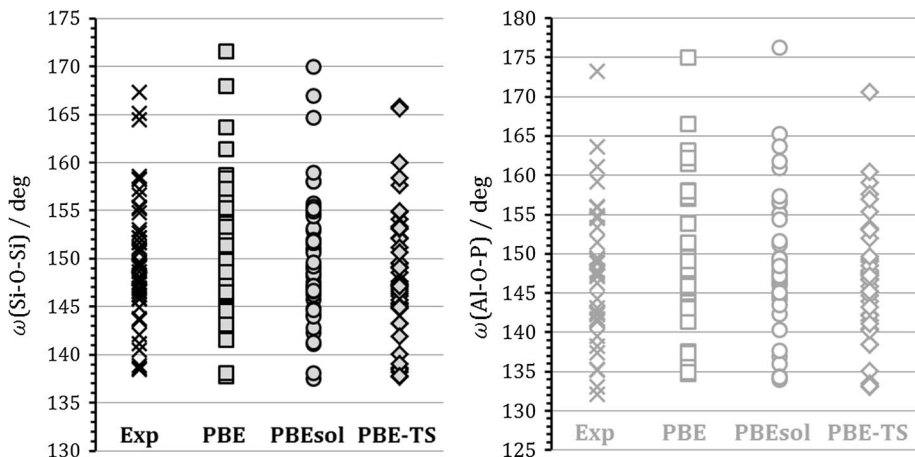
As mentioned above, a correction of the Si–O bond lengths for thermal motion leads to an increase by approximately 0.005 Å with respect to the “apparent” (= experimentally measured) bond length for structures obtained at room temperature [80]. While a detailed assessment of this effect by means of an analysis of the atomic displacement parameters is beyond the scope of the present work, it can be anticipated that the average error of the DFT methods would be reduced further if such a correction was applied.

The average Si–O–Si and Al–O–P bond angles and the values of *MSE*, *MAE*, and *LSE* for the different functionals

**Table 4** Average Si–O–Si and Al–O–P angles, overall errors in absolute terms (*MSE*, *MAE*) and largest signed errors (*LSE*) found among the individual results

	Exp	PBE	WC	PBEsol	PBE-D2	PBE-TS
Si–O–Si angles						
$\omega_{\text{aver}}/\text{deg}$	149.86	151.12	150.97	150.36	148.17	148.07
<i>MSE</i> /deg	–	+1.26	+1.11	+0.50	–1.69	–1.79
<i>MAE</i> /deg	–	2.09	2.02	1.49	2.62	2.46
<i>LSE</i> /deg	–	+6.12	+6.63	–5.43	–8.81	–9.05
Al–O–P angles						
$\omega_{\text{aver}}/\text{deg}$	147.48	149.24	149.22	148.83	147.31	146.82
<i>MSE</i> /deg	–	+1.76	+1.74	+1.35	–0.17	–0.66
<i>MAE</i> /deg	–	2.94	3.05	2.68	2.45	2.60
<i>LSE</i> /deg	–	+7.33	–6.97	–7.10	+7.45	+7.39

**Fig. 5** Distribution of T–O–T angles among all zeotypes considered. *Left* Si–O–Si angles in all-silica zeolites. *Right* Al–O–P angles in aluminophosphates



are compiled in Table 4. The distribution of the bond angles in the experimental structures is compared to the analogous distributions in the DFT-optimised structures obtained with PBE, PBEsol, and PBE-TS in Fig. 5 (again, results for WC and PBE-D2 are omitted), and the overall errors are visualised in Fig. 6.

In a given structure, the equilibrium T–O–T angle depends not only on the electronic configuration of the central oxygen atom, but also on the structural environment (size and shape of building units and windows in the vicinity). Thus, a rather large variation of the angles is observed in the experimental structures, with the Si–O–Si angles ranging from 138 to 167° and the Al–O–P angles ranging from 132 to 173°. The average values amount to 149.9 and 147.5°, respectively. A comparison of the average angles delivered by the different DFT approaches shows that the functionals without dispersion correction typically predict somewhat larger angles than experiment, whereas the dispersion-corrected approaches give smaller angles. This behaviour, which is in line with the observations of a recent study of zeolite MFI with the PBE and PBE-D2 functionals [38], is also reflected in the values of *MSE*: while the mean of signed errors is positive for PBE, WC, and PBEsol, it

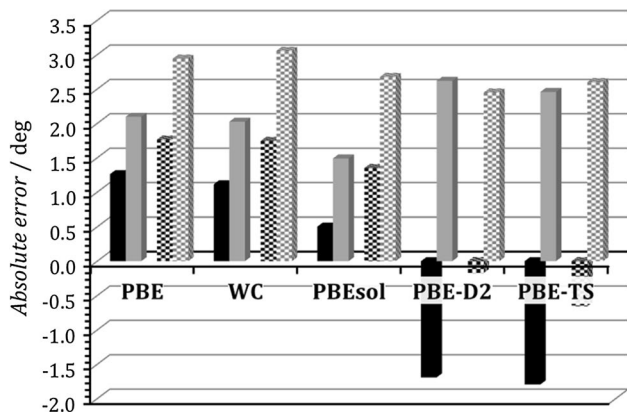


**Fig. 6** *MSE* and *MAE* in T–O–T angles. For each functional, the bars represent (from left to right): *MSE* (black, filled) and *MAE* (grey, filled) for Si–O–Si angles, *MSE* (black, checkered) and *MAE* (grey, checkered) for Al–O–P angles

has negative values for PBE-D2 and PBE-TS. The overall deviation is fairly similar for all functionals: for Si–O–Si angles, PBEsol performs best, with an *MAE* of 1.5° compared to *MAEs* above 2° for all other functionals, but its performance for Al–O–P angles is less impressive. Here, all

*MAE* values fall between roughly 2.5 and 3°. No functional predicts all T–O–T angles within  $\pm 5^\circ$  of the experimental values, with the largest individual errors approaching  $-10^\circ$ .

The qualitatively different behaviour of the functionals with and without dispersion correction can be understood from geometric considerations: As stated above, the equilibrium value of a given T–O–T angle will be strongly influenced by the interactions between the building units on both sides, i.e. between atoms that are not bonded to each other, but interact through long-range interactions. In a simple qualitative assessment, one can consider only the T atoms that are bonded to the central oxygen atom, neglecting the remainder of the structural environment. These atoms will be roughly 3 Å apart, a distance for which a significant dispersion interaction will be calculated in pairwise dispersion correction schemes. Because of this attractive dispersion contribution, the equilibrium distance between the T atoms will be optimised towards smaller values if a dispersion correction is applied, consequently leading to a smaller equilibrium T–O–T angle. On the other hand, pure-GGA functionals, which do not account for dispersion interactions, will neglect the attraction between these atoms, thus predicting larger angles. The observed behaviour of both PBE-D2 and PBE-TS indicates that the contribution of dispersion interactions is overestimated by these approaches, a finding that mirrors the observations of some previous benchmarking works [29, 83]. Thus, it appears likely that more evolved dispersion correction schemes incorporating “beyond pairwise” effects may be necessary to accurately capture the intricate balance of short-range and long-range interactions that govern the T–O–T angles [84–86].

### 3.3 Comparison to other methods I: B3LYP-D2 calculations

The structures of a total of 163 all-silica zeolites were fully optimised with the B3LYP-D2 functional in the work of Coudert, who then used further DFT calculations to predict the elastic properties of a subset of 121 zeolites [3]. Unlike the present plane-wave DFT study, these calculations employed the CRYSTAL code, which uses a local basis set with Gaussian-type basis functions [87]. Since all eight all-silica zeolites considered here were also included in Coudert’s work, we can assess the performance of the hybrid B3LYP functional with a Grimme-type dispersion correction in an analogous manner to the error analysis carried out for the GGA-type functionals. In Table 5, the overall errors of B3LYP-D2 in lattice parameters, Si–O bond lengths, and Si–O–Si angles are given. A direct comparison of the *MSE* and *MAE* in lattice parameters to those obtained with PBE, PBEsol, and PBE-TS is made in Fig. 6. While we have to note that  $\alpha$ -quartz was not included in the

**Table 5** Errors in lattice parameters, Si–O bond lengths, and Si–O–Si angles obtained with DFT calculations using the hybrid B3LYP-D2 functional [3] and with molecular mechanics calculations employing the SLC and ClayFF force fields

Lattice parameters	B3LYP-D2	SLC	ClayFF
<i>MSE</i> /Å	0.306	−0.051	−0.001
<i>MAE</i> /Å	0.306	0.074	0.070
<i>RMSE</i> /%	2.50	0.84	0.92
<i>LSE</i> /Å	+0.582 ( <i>b</i> , TON)	−0.226 ( <i>c</i> , SAS)	−0.233 ( <i>a</i> , IFR)
<i>LRE</i> /%	+4.83 ( <i>c</i> , TON)	−2.22 ( <i>c</i> , SAS)	2.42 ( <i>c</i> , TON)
Si–O bonds			
$d_{\text{aver}}$ /Å	1.616	1.601	1.576
<i>MSE</i> /Å	+0.015	0.000	−0.025
<i>MAE</i> /Å	0.016	0.007	0.025
<i>LSE</i> /Å	+0.039	−0.046	−0.062
Si–O–Si angles			
$\omega_{\text{aver}}$ /deg	157.57	148.29	159.41
<i>MSE</i> /deg	7.58	−1.57	9.54
<i>MAE</i> /deg	8.28	2.43	9.86
<i>LSE</i> /deg	31.57	−10.71	31.53

Error calculations comprised eight all-silica zeolites in the case of B3LYP-D2, and eight all-silica zeolites plus  $\alpha$ -quartz for the force fields

B3LYP-D2 calculations, a direct comparison of the overall errors is nevertheless meaningful because the omission of this system affects the values of *MSE* and *MAE* of the GGA-type functionals only marginally.

It is apparent that the B3LYP-D2 functional has a tendency to drastically overestimate the lattice parameters, with both absolute and relative errors that exceed those of the worst-performing GGA-type functional, PBE, by up to a factor of two. While the Si–O bond distances are also overestimated, the typical errors remain in the same range as for PBE and its dispersion-corrected variants. As for the lattice parameters, the errors in the angles are much larger than for all GGA-type functionals, with *MSE* and *MAE* exceeding 7.5°. An inspection of the individual results shows that deviations of more than 10° are not uncommon.

While the largest signed error in Si–O–Si angles found among the results exceeds 30°, it has to be pointed out that the most remarkable deviations occur for FER and TON, frameworks where the symmetry of the aristotype, rather than the experimentally observed symmetry, was used in the B3LYP-D2 calculations. Therefore, some angles are 180° for symmetry reasons, being very different from the experimentally measured angles (one example is the Si1–O8–Si2 angle in FER, mentioned above). While these symmetry constraints on some of the T–O–T angles will also



affect the predicted equilibrium lattice parameters, a closer look at the individual results reveals that even an exclusion of FER and TON reduces the overall *MAE/MSE* in lattice parameters of B3LYP-D2 only marginally.

It has to be conceded that the comparability of the B3LYP-D2 results to those of the present work is intrinsically limited due to the use of different types of basis sets, in particular as the quality of the Gaussian-type basis set has a rather strong impact on the resulting structures. In their study of all-silica zeolites, Román-Román and Zicovich-Wilson [34] found considerable changes in the molar volume (up to a few per cent) when moving from a small to a fairly large (triple-zeta) Gaussian-type basis set. Even with the larger basis set, these authors observed a significant overestimation of the molar volume when using the B3LYP functional in conjunction with a dispersion correction. This finding, taken together with the above analysis of the structures from [3], clearly indicates that the observed tendency of B3LYP-D2 to overestimate the lattice dimensions is systematic. Nevertheless, further plane-wave calculations with this functional would be necessary to enable a fully quantitative comparison to the results of the present work. While the computational overhead that comes with the inclusion of a fraction of exact exchange does not appear to be justified for the case of B3LYP, it has to be emphasised that this finding cannot be generalised to other hybrid functionals. For example, the PBE0 functional has been used rather successfully in some computational studies of zeolite structures [27, 35].

### 3.4 Comparison to other methods II: molecular mechanics calculations

Molecular mechanics calculations are computationally much less expensive than DFT calculations, and various force fields designed for all-silica polymorphs have been devised (see [88] for a comprehensive overview). Naturally, the question arises whether the use of computationally demanding DFT methods is actually needed to arrive at an accurate prediction of the structure of all-silica zeolites, or whether a well-calibrated force field might be able to deliver results of similar (or even better) accuracy. While this aspect cannot be addressed in full within the context of this work, an initial assessment was made, performing additional molecular mechanics calculations employing two widely used force fields: firstly, the force field developed by Sanders, Leslie, and Catlow (SLC) [89], which uses core-shell potentials, and secondly, the more recently developed ClayFF force field [90], which employs a combination of point charges and Lennard-Jones potentials. In a comparative study of 16 different force fields, SLC was found to rank among the best-performing force fields

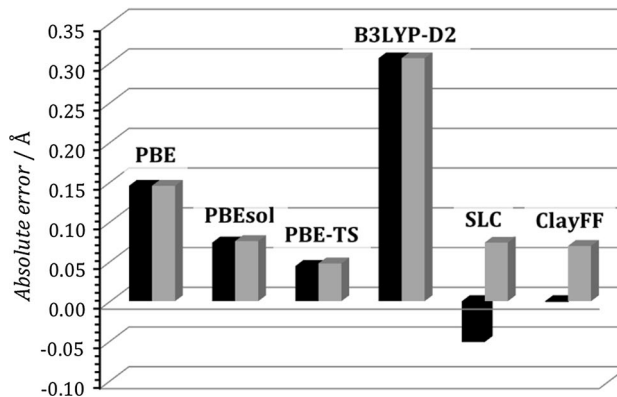


**Fig. 7** Comparison of the performance of three GGA-type functionals to the hybrid B3LYP-D2 functional (results from Coudert’s work [3]) and to two force fields (SLC and ClayFF): *MSE* (black) and *MAE* (grey) in lattice parameters for all-silica systems

for the structure optimisation of eight-ring zeolites and dense  $\text{SiO}_2$  polymorphs [88]. ClayFF, which was primarily designed for clays and related layered materials, was included in the present work due to its broad applicability.

The overall errors obtained with these two force fields are included in Table 5, and, for lattice parameters, a comparison to some of the GGA-type functionals is made in Fig. 7. Both force fields predict the lattice parameters with an overall accuracy that is comparable to the PBEsol functional, performing significantly better than PBE, but worse than PBE-TS and PBE-D2. An inspection of the mean of signed errors shows that, in contrast to the DFT approaches, the force fields do not exhibit a systematic tendency to overestimate the lattice parameters: While SLC tends to deliver too small lattice dimensions, the *MSE* for ClayFF is practically zero, i.e. over- and underpredictions cancel each other out.

With regard to the Si–O bond lengths, SLC outperforms all DFT approaches, predicting an average Si–O distance that is in excellent agreement with experiment and delivering very small values of *MSE* and *MAE*. In this context, it is worth noting that the SLC force field was calibrated on room-temperature structures of  $\text{SiO}_2$  polymorphs ( $\alpha$ -quartz,  $\alpha$ -cristobalite,  $\alpha$ -tridymite, coesite). While the good agreement for the bond lengths is, therefore, not entirely unexpected, the transferability of this force field is nevertheless impressive. The typical errors of SLC in the Si–O–Si angles are similar to those of the dispersion-corrected variants of PBE, and the predicted average angle is also somewhat smaller than the experimental value. As for PBE-D2 and PBE-TS, this might point to an overestimation of long-range interactions between atoms that are not bonded to each other. In contrast to the good performance of SLC, ClayFF underestimates the Si–O bond lengths significantly,

with average deviations in the range of 0.025 Å. The deviations in the Si–O–Si angles are also very large and exceed those of B3LYP-D2. In some instances, a ClayFF optimisation leads to a final structure in which some Si–O–Si angles equal 180°: for example, an optimisation of FER that starts from the experimental structure (space group  $Pm\bar{3}n$ , no linearly coordinated oxygen atoms) delivers a final structure with  $Im\bar{3}m$  symmetry and an Si1–O8–Si2 angle of 180°. Overall, the performance of ClayFF is not satisfactory, despite the small *MSE* and *MAE* values found for the lattice parameters.

### 3.5 Discussion of outliers: all-silica SOD and AST

As mentioned previously, rather large deviations between DFT-optimised and experimental structures were found for two all-silica zeolites that were initially included in the set of systems studied, all-silica SOD and AST. As the errors observed for these two systems appear to be systematic and intricately linked to particular structural features, they were omitted from the overall error analysis presented above. Instead, key findings for SOD and AST are discussed separately in this section.

As an initial remark, it is important to note that the symmetry of the experimentally observed structures are reduced with respect to the aristotype of the SOD and AST frameworks, both of which are cubic. In the case of SOD, the experimental structure has rhombohedral symmetry, and the reduction of the symmetry manifests in a distortion of the sodalite (*sod*) cages [78]: while the two six-ring windows that lie perpendicular to the *c*-axis retain a regular hexagonal shape, the other six windows are heavily distorted (Fig. 8). Similarly, all 12 six-ring windows bordering the *ast* cage are equivalent in the cubic aristotype of the AST structure, whereas there are two distinct types of six-ring windows in the experimentally observed, tetragonal structure [77]. Here, in particular the six-rings that lie perpendicular to  $\langle 100 \rangle$  are fairly distorted.

For SOD, the GGA functionals without dispersion correction overestimate the lattice dimensions, with errors in *a* amounting to roughly 0.2 Å (~1.5%), and errors in *c* reaching up to 0.4 Å (~6%). The two dispersion-corrected variants give a good prediction of *a*, but underestimate *c* by up to 0.2 Å (~3%). While the pure-GGA functionals overestimate the Si–O–Si angles at both oxygen atoms by ~5° or more, PBE-D2 and PBE-TS underestimate them by a slightly smaller amount. The qualitatively different behaviour of the functionals with and without dispersion correction can be understood from a closer look at the *sod* cage, and especially those six-ring windows that are distorted in the rhombohedral structure. Figure 8 visualises this building unit in the experimentally determined structure and in the DFT-optimised structures obtained with PBEsol and PBE-TS. Relevant atom–atom distances across the

window are included in the figure. It is apparent that the window is less distorted in the PBEsol structure than in the experimental structure, whereas the distortion is exaggerated by PBE-TS. These changes in the window distortion also explain the observed trends in the lattice parameters. In line with previously discussed observations, this behaviour can be attributed to the crucial role of dispersion interactions: Since the pure-GGA functionals do not account for dispersion, the weak attractive forces acting between atoms across the window, which stabilise the distortion, are absent, and the optimisation with any of these functionals reduces the distortion. Conversely, PBE-D2 and PBE-TS overestimate the long-range attraction across the window, thus predicting an even stronger distortion than observed experimentally.

In the case of AST, pure-GGA functionals overpredict *a* by up to 0.2 Å (~2%), and overestimate the Si1–O3–Si2 angle by a significant amount (while the other two angles are predicted rather accurately). The dispersion-corrected approaches deliver too small values of *a* and too large values of *c*, and both the Si1–O2–Si1 angle and the Si1–O3–Si2 angle are underestimated. Again, this behaviour can be explained by looking at the distorted six-ring windows of the *ast* cage, visualised in Fig. 8. As in the case of SOD, PBEsol and other variants without dispersion correction deliver an equilibrium structure that is slightly less distorted than the experimental one, whereas PBE-TS (and PBE-D2) lead to a larger distortion. The same explanation based on the absence/overestimation of dispersion interaction can be invoked here. Since those six-rings for which the distortion is most pronounced lie perpendicular to  $\langle 100 \rangle$ , the observed changes in unit cell dimensions in structures optimised with dispersion-corrected DFT (shrinkage along *a*, extension along *c*, Table 6) are directly correlated with the increased distortion of these six-rings.

### 3.6 Relative stability of selected SiO<sub>2</sub> frameworks

While the present work is primarily targeted at obtaining accurate structures, it is quite useful to also include some energetic considerations. Therefore, the relative stability of SiO<sub>2</sub> zeolites was assessed for those systems from the set of reference structures for which experimental data are available. The relative stability is calculated as the difference between the DFT energies (per formula unit SiO<sub>2</sub>) obtained for a given zeolite and for  $\alpha$ -quartz, the thermodynamically stable SiO<sub>2</sub> polymorph at ambient conditions. In keeping with previous studies, the difference of the DFT energies  $\Delta E_{\text{DFT}}$  is directly compared to the experimental enthalpy of transition from  $\alpha$ -quartz to the zeolite,  $\Delta H_{\text{exp}}$ , thereby ignoring vibrational contributions [34]. For those zeolites for which experimental enthalpy data are available (CHA, FAU, FER, IFR), Table 7 provides values of  $\Delta H_{\text{exp}}$  (from

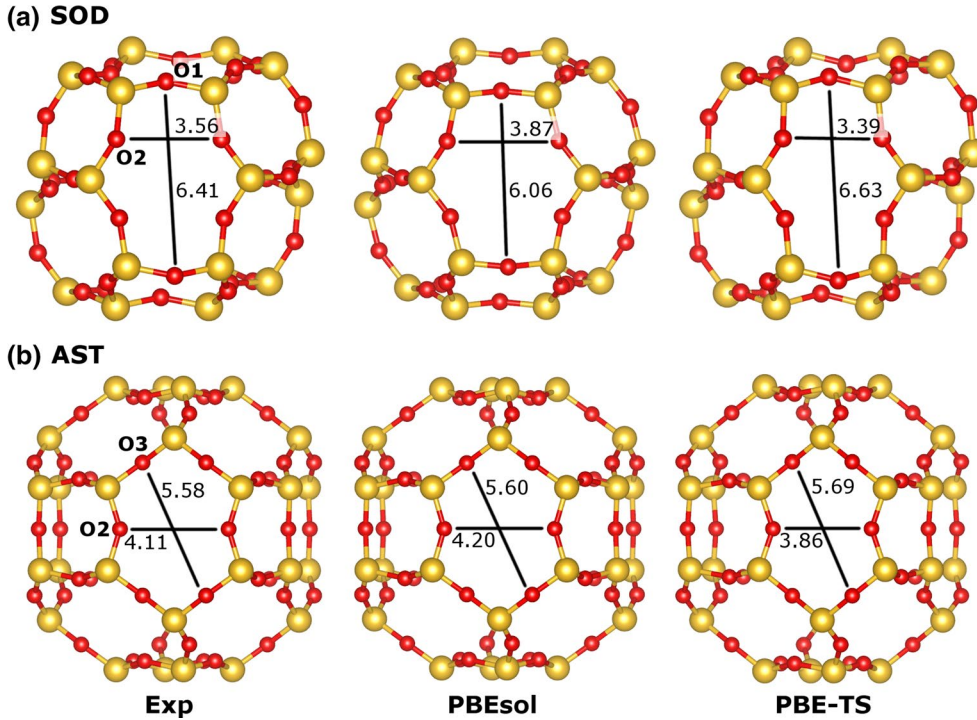


**Fig. 8** Visualisation of the *sod* cage in SOD and the *ast* cage in AST, comparing the experimental structures to those optimised with PBEsol and PBE-TS functionals. Selected oxygen–oxygen distances across the six-ring windows are given (in Å)

**Table 6** Comparison of lattice parameters and T–O–T angles obtained in DFT optimisations to experimental values for all-silica SOD and AST

	Exp	PBE	WC	PBEsol	PBE-D2	PBE-TS
SOD						
$a/\text{Å}$	12.441	12.655	12.618	12.597	12.442	12.411
$c/\text{Å}$	7.091	7.515	7.505	7.411	6.915	6.898
$\omega(\text{Si1-O1-Si1})/\text{deg}$	149.02	156.20	157.99	155.90	145.73	144.40
$\omega(\text{Si1-O2-Si1})/\text{deg}$	145.93	152.90	152.72	150.64	141.74	142.49
AST						
$a/\text{Å}$	9.255	9.446	9.418	9.387	9.115	9.066
$c/\text{Å}$	13.501	13.621	13.561	13.556	13.739	13.757
$\omega(\text{Si1-O1-Si1})/\text{deg}$	147.22	147.85	147.83	147.65	149.74	150.03
$\omega(\text{Si1-O2-Si1})/\text{deg}$	146.54	147.31	147.32	147.50	143.03	142.18
$\omega(\text{Si1-O3-Si2})/\text{deg}$	151.74	157.55	158.44	156.23	145.89	144.93

[91]) and  $\Delta E_{\text{DFT}}$  obtained with the PBE-D2 and PBE-TS functionals. Results with pure-GGA functionals are omitted, as these functionals give very small values of  $\Delta E_{\text{DFT}}$  (below 3 kJ mol<sup>-1</sup> in all cases). This observation corroborates the previous finding that the inclusion of a dispersion correction is crucial to arrive at a reasonable quantitative prediction of the relative stability [34]. The two dispersion-corrected variants give the correct order of stability ( $\alpha$ -quartz–FER–IFR–CHA–FAU); however, the PBE-TS functional overestimates the energy difference by 30–100%. PBE-D2 delivers a much better prediction, with near-quantitative agreement

for three of the four systems. This finding might appear somewhat surprising given the previous observation that the Grimme-type D2 dispersion correction typically tends to overestimate the dispersion contribution in periodic systems, because the dispersion coefficients were derived for molecules, not for solids (see e.g. the discussion in [29]). It can thus be hypothesised that the good performance of PBE-D2 is, to some extent, owed to a cancellation of errors: The much too small  $\Delta E_{\text{DFT}}$  obtained by PBE alone is compensated by an overestimated dispersion contribution. While the good agreement between calculations and experiment

**Table 7** Comparison of the differences of the DFT energies with respect to  $\alpha$ -quartz ( $\Delta E_{\text{DFT}}$ ) to experimental enthalpies of transition ( $\Delta H_{\text{exp}}$ )

	$\Delta H_{\text{exp}}$	$\Delta E_{\text{DFT}}$ (PBE-D2)	$\Delta E_{\text{DFT}}$ (PBE-TS)
CHA	11.4	12.1	17.2
FAU	13.6	12.8	17.9
FER	6.6	9.1	13.0
IFR	10.0	10.3	14.3

Only all-silica systems for which experimental data are available are included. All values are given in  $\text{kJ mol}^{-1}$ , with errors in the experimental values (where reported) being in the range of  $1.0 \text{ kJ mol}^{-1}$

may be somewhat fortuitous, it would be insightful to study the performance of the PBE-D2 functional in the prediction of relative stabilities of zeotypes in more depth.

## 4 Conclusions

The key results of our benchmarking of DFT-GGA for the structure optimisation of neutral-framework zeotypes can be summarised as follows:

1. The well-known overestimation of lattice parameters by PBE is only partially cured in GGA-type functionals for solids, WC and PBEsol, which still exhibit a systematic tendency to overestimate the lattice dimensions. Dispersion-corrected variants of PBE perform significantly better than the uncorrected functionals, with PBE-TS giving particularly good results. It can be concluded that some means to account for dispersion interactions is pivotal to obtain accurate lattice parameters in these framework compounds. Interestingly, PBE-TS outperforms PBEsol and WC even for the dense frameworks,  $\alpha$ -quartz and  $\alpha$ -berlinite. This observation, together with the previous findings of the benchmarking study of Tran et al. [18], might call for a more systematic study of the performance of dispersion-corrected DFT for dense solids.
2. PBE tends to deliver moderately too long T–O bond lengths, and this behaviour is not affected by the dispersion correction. Since WC and PBEsol give more accurate bond distances, it could be fruitful to combine these functionals with a dispersion correction in future work.
3. Unlike for lattice parameters and bond distances, none of the functionals considered gives completely satisfactory agreement for T–O–T angles. While the pure-GGA functionals tend to give larger angles than observed experimentally, the dispersion-corrected functionals deliver too small angles. This behaviour is likely to result from an overestimation of dispersion

interactions between atoms that are relatively close together without being directly bonded to each other. This problem was also identified as the origin of the rather poor performance of dispersion-corrected DFT for two outliers that were removed from the set of reference structures, SOD and AST. In these frameworks, both PBE-D2 and PBE-TS exaggerate the distortion of certain windows, leading to rather large errors in the predicted lattice parameters.

4. A comparison with two widely used force fields shows that PBE-TS, the best-performing functional, delivers more accurate results than SLC, the better of the two force fields. However, the performance is not massively superior, indicating that well-calibrated force fields remain competitive to dispersion-corrected DFT. It thus depends on the task in question whether the computational overhead of DFT is justified or not. With increasing computational power, however, it becomes easier to use DFT routinely for task that were previously addressed with force field methods, e.g. to optimise structure models of zeotypes for which a full refinement from experimental diffraction data is not possible.
5. The relative stability of all-silica zeolites with respect to  $\alpha$ -quartz is predicted fairly accurately by the PBE-D2 functional, at least for the limited number of frameworks for which experimental enthalpies are available. While the inclusion of dispersion corrections is absolutely necessary to arrive at realistic energy differences, PBE-TS, the best-performing functional for structural properties, performs considerably worse than PBE-D2. The good performance of the PBE-TS functional in the prediction of structures, but its rather poor performance for energetics, is in line with the observations made in previous studies of molecular crystals: although PBE-TS delivers accurate structures [12], it was found that a combination of optimisations at the PBE-TS level with single-point calculations employing the PBE0 functional and incorporating many-body dispersion (MBD) effects was necessary to arrive at sufficiently accurate lattice energies [11, 86]. The very successful submission of Tkatchenko et al. to the Sixth Blind Test of Organic Crystal Structure Prediction Methods used this approach [92].

Altogether, the accuracy obtained with dispersion-corrected GGA functionals is very encouraging. In particular, the PBE-TS approach, which is more sophisticated and less empirical than PBE-D2, can be recommended as a reasonable default choice for structure optimisations, although additional care should be taken in cases where peculiar structural distortions play a role. Clearly, the results of the present study have also shown that there is space for further



improvement, especially in terms of the accurate representation of dispersion interactions. It will thus be useful to assess a wider range of functionals and dispersion correction schemes in due course. However, as it has been highlighted throughout the discussion, the interpretation of the observed accuracy remains somewhat “fuzzy” due to the inherent differences between the DFT-optimised structures, corresponding to 0 K, and the experimental structures, which were obtained at finite temperatures (mostly room temperature). In particular, the average errors in lattice parameters of the best-performing PBE-TS functional approach the (estimated) difference between 0 K and room-temperature lattice dimensions. Consequently, a more exact assessment of the deviations between DFT-optimised and experimental structures would require further experimental work comprising structure refinements on low-temperature datasets.

Finally, it has to be noted that only neutral-framework zeotypes were included in the present study, whereas proton- or cation-exchanged systems are more relevant for many applications (e.g. in catalysis or separation). While it can be expected that the main findings of this work should be transferable to charged-framework zeotypes (aluminosilicates, silicoaluminophosphates, etc.), further testing would be necessary. As many of these materials exhibit fractionally occupied cation sites or mixed occupancies on T sites, the construction of representative structure models that can be used in DFT calculations remains a particular challenge.

**Acknowledgements** M. F. and F. O. E. are grateful to Prof. Dr Andreas Lüttge and Dr Rolf Arvidson (Marum, Bremen) for generous access to the Asgard cluster, on which the DFT calculations were run. We would like to thank Dr FX Coudert (CNRS, ParisTech) for sharing the B3LYP-D2 structures with us, as well as Dr Ross Angel (Padova) for insightful discussions. M. F. is funded by the Central Research Development Funds (CRDF) of the University of Bremen (Funding line 04—Independent Projects for Post-Docs). F. F. and A. O. are grateful for support by the Wrocław Centre for Networking and Supercomputing (grant no. 172), providing access to the BIO-VIA *Materials Studio* 8.0 software.

## References

- Masters AF, Maschmeyer T (2011) Zeolites—from curiosity to cornerstone. *Microporous Mesoporous Mater* 142:423–438. doi:10.1016/j.micromeso.2010.12.026
- Van Speybroeck V, Hemelsoet K, Joos L, Waroquier M, Bell RG, Catlow CRA (2015) Advances in theory and their application within the field of zeolite chemistry. *Chem Soc Rev* 44:7044–7111. doi:10.1039/C5CS00029G
- Coudert F-X (2013) Systematic investigation of the mechanical properties of pure silica zeolites: stiffness, anisotropy, and negative linear compressibility. *Phys Chem Chem Phys* 15:16012–16018. doi:10.1039/c3cp51817e
- Fischer M, Bell RG (2013) Identifying promising zeolite frameworks for separation applications: a building-block-based approach. *J Phys Chem C* 117:17099–17110. doi:10.1021/jp405507y
- Johnson ER, Mackie ID, DiLabio GA (2009) Dispersion interactions in density-functional theory. *J Phys Org Chem* 22:1127–1135. doi:10.1002/poc.1606
- Eshuis H, Furche F (2011) A parameter-free density functional that works for noncovalent interactions. *J Phys Chem Lett* 2:983–989. doi:10.1021/jz200238f
- Grimme S (2011) Density functional theory with London dispersion corrections. *Wiley Interdiscip Rev Comput Mol Sci* 1:211–228. doi:10.1002/wcms.30
- Grimme S, Hansen A, Brandenburg JG, Bannwarth C (2016) Dispersion-corrected mean-field electronic structure methods. *Chem Rev* 116:5105–5154. doi:10.1021/acs.chemrev.5b00533
- Goerigk L, Kruse H, Grimme S (2011) Benchmarking density functional methods against the S66 and S66x8 datasets for non-covalent interactions. *ChemPhysChem* 12:3421–3433. doi:10.1002/cphc.201100826
- Risthaus T, Grimme S (2013) Benchmarking of London dispersion-accounting density functional theory methods on very large molecular complexes. *J Chem Theory Comput* 9:1580–1591. doi:10.1021/ct301081n
- Reilly AM, Tkatchenko A (2013) Understanding the role of vibrations, exact exchange, and many-body van der Waals interactions in the cohesive properties of molecular crystals. *J Chem Phys* 139:024705. doi:10.1063/1.4812819
- Binns J, Healy MR, Parsons S, Morrison CA (2014) Assessing the performance of density functional theory in optimizing molecular crystal structure parameters. *Acta Crystallogr Sect B Struct Sci Cryst Eng Mater* 70:259–267. doi:10.1107/S205252061303268X
- Carter DJ, Rohl AL (2014) Benchmarking calculated lattice parameters and energies of molecular crystals using van der Waals density functionals. *J Chem Theory Comput* 10:3423–3437. doi:10.1021/ct500335b
- Remya K, Suresh CH (2013) Which density functional is close to CCSD accuracy to describe geometry and interaction energy of small non-covalent dimers? A benchmark study using Gaussian09. *J Comput Chem* 34:1341–1353. doi:10.1002/jcc.23263
- Perdew JP, Burke K, Ernzerhof M (1996) Generalized gradient approximation made simple. *Phys Rev Lett* 77:3865–3868. doi:10.1103/PhysRevLett.77.3865
- Tran F, Laskowski R, Blaha P, Schwarz K (2007) Performance on molecules, surfaces, and solids of the Wu–Cohen GGA exchange-correlation energy functional. *Phys Rev B* 75:115131. doi:10.1103/PhysRevB.75.115131
- Haas P, Tran F, Blaha P (2009) Calculation of the lattice constant of solids with semilocal functionals. *Phys Rev B* 79:085104. doi:10.1103/PhysRevB.79.085104
- Tran F, Stelzl J, Blaha P (2016) Rungs 1 to 4 of DFT Jacob’s ladder: extensive test on the lattice constant, bulk modulus, and cohesive energy of solids. *J Chem Phys* 144:204120. doi:10.1063/1.4948636
- Wu Z, Cohen R (2006) More accurate generalized gradient approximation for solids. *Phys Rev B* 73:235116. doi:10.1103/PhysRevB.73.235116
- Perdew J, Ruzsinszky A, Csonka G, Vydrov O, Scuseria G, Constantin L, Zhou X, Burke K (2008) Restoring the density-gradient expansion for exchange in solids and surfaces. *Phys Rev Lett* 100:136406. doi:10.1103/PhysRevLett.100.136406
- Constantin LA, Terentjevs A, Della Sala F, Cortona P, Fabiano E (2016) Semiclassical atom theory applied to solid-state physics. *Phys Rev B* 93:045126. doi:10.1103/PhysRevB.93.045126

22. Grimme S (2006) Semiempirical GGA-type density functional constructed with a long-range dispersion correction. *J Comput Chem* 27:1787–1799. doi:10.1002/jcc.20495
23. Grimme S, Antony J, Ehrlich S, Krieg H (2010) A consistent and accurate ab initio parametrization of density functional dispersion correction (DFT-D) for the 94 elements H–Pu. *J Chem Phys* 132:154104. doi:10.1063/1.3382344
24. Demichelis R, Civalleri B, Ferrabone M, Dovesi R (2010) On the performance of eleven DFT functionals in the description of the vibrational properties of aluminosilicates. *Int J Quantum Chem* 110:406–415. doi:10.1002/qua.22301
25. De la Pierre M, Orlando R, Maschio L, Doll K, Ugliengo P, Dovesi R (2011) Performance of six functionals (LDA, PBE, PBESOL, B3LYP, PBE0, and WC1LYP) in the simulation of vibrational and dielectric properties of crystalline compounds. The case of forsterite  $Mg_2SiO_4$ . *J Comput Chem* 32:1775–1784. doi:10.1002/jcc.21750
26. Demichelis R, Civalleri B, D’Arco P, Dovesi R (2010) Performance of 12 DFT functionals in the study of crystal systems:  $Al_2SiO_5$  orthosilicates and Al hydroxides as a case study. *Int J Quantum Chem* 110:2260–2273. doi:10.1002/qua.22574
27. Valdiviés Cruz K, Lam A, Zicovich-Wilson CM (2014) Periodic quantum chemical studies on anhydrous and hydrated acid clinoptilolite. *J Phys Chem A* 118:5779–5789. doi:10.1021/jp410754a
28. Pernot P, Civalleri B, Presti D, Savin A (2015) Prediction uncertainty of density functional approximations for properties of crystals with cubic symmetry. *J Phys Chem A* 119:5288–5304. doi:10.1021/jp509980w
29. Tunega D, Bučko T, Zaoui A (2012) Assessment of ten DFT methods in predicting structures of sheet silicates: importance of dispersion corrections. *J Chem Phys* 137:114105. doi:10.1063/1.4752196
30. Tkatchenko A, Scheffler M (2009) Accurate molecular Van Der Waals interactions from ground-state electron density and free-atom reference data. *Phys Rev Lett* 102:073005. doi:10.1103/PhysRevLett.102.073005
31. Adamo C, Barone V (1999) Toward reliable density functional methods without adjustable parameters: the PBE0 model. *J Chem Phys* 110:6158. doi:10.1063/1.478522
32. Becke AD (1993) Density-functional thermochemistry. III. The role of exact exchange. *J Chem Phys* 98:5648–5652. doi:10.1063/1.464913
33. Lee C, Yang W, Parr RG (1988) Development of the Colle-Salvetti correlation-energy formula into a functional of the electron density. *Phys Rev B* 37:785–789. doi:10.1103/PhysRevB.37.785
34. Román-Román EI, Zicovich-Wilson CM (2015) The role of long-range van der Waals forces in the relative stability of  $SiO_2$ -zeolites. *Chem Phys Lett* 619:109–114. doi:10.1016/j.cplett.2014.11.044
35. Göttl F, Hafner J (2012) Structure and properties of metal-exchanged zeolites studied using gradient-corrected and hybrid functionals. I. Structure and energetics. *J Chem Phys* 136:064501. doi:10.1063/1.3676408
36. Göttl F, Hafner J (2012) Structure and properties of metal-exchanged zeolites studied using gradient-corrected and hybrid functionals. II. Electronic structure and photoluminescence spectra. *J Chem Phys* 136:064502. doi:10.1063/1.3676409
37. Göttl F, Hafner J (2012) Structure and properties of metal-exchanged zeolites studied using gradient-corrected and hybrid functionals. III. Energetics and vibrational spectroscopy of adsorbates. *J Chem Phys* 136:064503. doi:10.1063/1.3676410
38. Hernandez-Tamargo CE, Roldan A, de Leeuw NH (2016) A density functional theory study of the structure of pure-silica and aluminium-substituted MFI nanosheets. *J Solid State Chem* 237:192–203. doi:10.1016/j.jssc.2016.02.006
39. Larin AV, Trubnikov DN, Vercauteren DP (2005) Improvement of X-ray diffraction geometries of water physisorbed in zeolites on the basis of periodic Hartree-Fock calculations. *Int J Quantum Chem* 102:971–979. doi:10.1002/qua.20463
40. Labat F, Fuchs AH, Adamo C (2010) Toward an accurate modeling of the Water – Zeolite Interaction: calibrating the DFT approach. *J Phys Chem Lett* 1:763–768. doi:10.1021/jz100011p
41. Fischer M (2015) Structure and bonding of water molecules in zeolite hosts: benchmarking plane-wave DFT against crystal structure data. *Z Kristallogr* 230:325–336. doi:10.1515/zkri-2014-1809
42. Uzunova EL, Göttl F, Kresse G, Hafner J (2009) Application of hybrid functionals to the modeling of NO adsorption on Cu – SAPO-34 and Co – SAPO-34: a periodic DFT study. *J Phys Chem C* 113:5274–5291. doi:10.1021/jp809927k
43. Otero Arean C, Delgado MR, Nachtigall P, Thang HV, Rubeš M, Bulánek R, Chlubná-Eliášová P (2014) Measuring the Brønsted acid strength of zeolites—does it correlate with the O–H frequency shift probed by a weak base? *Phys Chem Chem Phys* 16:10129–10141. doi:10.1039/c3cp54738h
44. Nour Z, Berthomieu D (2014) Multiple adsorption of CO on Na-exchanged Y faujasite: a DFT investigation. *Mol Simul* 40:33–44. doi:10.1080/08927022.2013.848281
45. Fischer M, Delgado MR, Areán CO, Duran CO (2015) CO adsorption complexes in zeolites: how does the inclusion of dispersion interactions affect predictions made from DFT calculations? The case of Na-CHA. *Theor Chem Acc* 134:91. doi:10.1007/s00214-015-1692-9
46. Shang J, Li G, Singh R, Xiao P, Danaci D, Liu JZ, Webley PA (2014) Adsorption of  $CO_2$ ,  $N_2$ , and  $CH_4$  in Cs-exchanged chabazite: a combination of van der Waals density functional theory calculations and experiment study. *J Chem Phys* 140:084705. doi:10.1063/1.4866455
47. Nguyen CM, Reyniers M-F, Marin GB (2010) Theoretical study of the adsorption of C1–C4 primary alcohols in H-ZSM-5. *Phys Chem Chem Phys* 12:9481–9493. doi:10.1039/c000503g
48. Göttl F, Hafner J (2011) Alkane adsorption in Na-exchanged chabazite: the influence of dispersion forces. *J Chem Phys* 134:064102. doi:10.1063/1.3549815
49. Van der Mynsbrugge J, Hemelsoet K, Vandichel M, Waroquier M, Van Speybroeck V (2012) Efficient approach for the computational study of alcohol and nitrile adsorption in H-ZSM-5. *J Phys Chem C* 116:5499–5508. doi:10.1021/jp2123828
50. Göttl F, Grüneis A, Bučko T, Hafner J (2012) Van der Waals interactions between hydrocarbon molecules and zeolites: periodic calculations at different levels of theory, from density functional theory to the random phase approximation and Møller–Plesset perturbation theory. *J Chem Phys* 137:114111. doi:10.1063/1.4750979
51. Göttl F, Hafner J (2013) Modelling the adsorption of short alkanes in protonated chabazite: the impact of dispersion forces and temperature. *Microporous Mesoporous Mater* 166:176–184. doi:10.1016/j.micromeso.2012.04.052
52. Chiu C, Vayssilov GN, Genest A, Borgna A, Rösch N (2014) Predicting adsorption enthalpies on silicalite and HZSM-5: a benchmark study on DFT strategies addressing dispersion interactions. *J Comput Chem* 35:809–819. doi:10.1002/jcc.23558
53. Göttl F, Sautet P (2014) Modeling the adsorption of short alkanes in the zeolite SSZ-13 using “van der Waals” DFT exchange correlation functionals: understanding the advantages and limitations of such functionals. *J Chem Phys* 140:154105. doi:10.1063/1.4871085
54. Plévert J, Okubo T, Kubota Y, Honda T, Sugi Y (2000) GUS-1: a mordenite-like molecular sieve with the 12-ring channel of ZSM-12. *Chem Commun* 2363–2364. doi:10.1039/b005225f
55. Vaughan PA (1966) The crystal structure of the zeolite ferrierite. *Acta Crystallogr* 21:983–990. doi:10.1107/S0365110X66004298

56. Pickering IJ, Maddox PJ, Thomas JM, Cheetham AK (1989) A neutron powder diffraction analysis of ferrierite. *J Catal* 265:261–265
57. Alberti A, Sabelli C (1987) Statistical and true symmetry of ferrierite: possible absence of straight T–O–T bridging bonds. *Zeitschrift für Krist* 178:249–256. doi:10.1524/zkri.1987.178.1-4.249
58. Morris RE, Weigel SJ, Henson NJ, Bull LM, Janicke MT, Chmelka BF, Cheetham AK (1994) A synchrotron X-ray diffraction, neutron diffraction,  $^{29}\text{Si}$  MAS-NMR, and computational study of the siliceous form of zeolite ferrierite. *J Am Chem Soc* 116:11849–11855. doi:10.1021/ja00105a027
59. Lewis JE, Freyhardt CC, Davis ME (1996) Location of pyridine guest molecules in an electroneutral  $\{3\infty\}[\text{SiO}_{4/2}]$  host framework: single-crystal structures of the as-synthesized and calcined forms of high-silica ferrierite. *J Phys Chem* 100:5039–5049. doi:10.1021/jp9530055
60. Baur WH, Fischer RX (2010) ZeoBase—a databank for zeolite-type crystal structures. In: De Frede A (ed) Proceedings of the 16th International Zeolite Conference, Sorrento, Italy
61. Baerlocher C, McCusker LB (2012) Database of zeolite structures. <http://www.iza-structure.org/databases/>
62. Clark SJ, Segall MD, Pickard CJ, Hasnip PJ, Probert MIJ, Refson K, Payne MC (2005) First principles methods using CASTEP. *Z Kristallogr* 220:567–570. doi:10.1524/zkri.220.5.567.65075
63. Francis GP, Payne MC (1990) Finite basis set corrections to total energy pseudopotential calculations. *J Phys: Condens Matter* 2:4395–4404. doi:10.1088/0953-8984/2/19/007
64. Kihara K (1990) An X-ray study of the temperature dependence of the quartz structure. *Eur J Mineral* 2:63–78. doi:10.1127/ejm/2/1/0063
65. Onac BP, Effenberger HS (2007) Re-examination of berlinite ( $\text{AlPO}_4$ ) from the Cioclovina Cave, Romania. *Am Mineral* 92:1998–2001. doi:10.2138/am.2007.2581
66. Díaz-Cabañas M-J, Barrett PA, Cambor MA (1998) Synthesis and structure of pure  $\text{SiO}_2$  chabazite: the  $\text{SiO}_2$  polymorph with the lowest framework density. *Chem Commun* 1881–1882. doi:10.1039/a804800b
67. Hriljac JA, Eddy MM, Cheetham AK, Donohue JA, Ray GJ (1993) Powder neutron diffraction and  $^{29}\text{Si}$  MAS NMR studies of siliceous zeolite-Y. *J Solid State Chem* 106:66–72. doi:10.1006/jssc.1993.1265
68. Villaescusa LA, Lightfoot P, Teat SJ, Morris RE (2001) Variable-temperature microcrystal X-ray diffraction studies of negative thermal expansion in the pure silica zeolite IFR. *J Am Chem Soc* 123:5453–5459. doi:10.1021/ja015797o
69. Corma A, Rey F, Rius J, Sabater MJ, Valencia S (2004) Supramolecular self-assembled molecules as organic directing agent for synthesis of zeolites. *Nature* 431:287–290. doi:10.1038/nature02909
70. Marler B, Grünwald-Lüke A, Gies H (1998) Structure refinement of the as-synthesized and the calcined form of zeolite RUB-3 (RTE). *Microporous Mesoporous Mater* 26:49–59. doi:10.1016/S1387-1811(98)00213-3
71. Wragg DS, Morris R, Burton AW, Zones SI, Ong K, Lee G (2007) The synthesis and structure of SSZ-73: an all-silica zeolite with an unusual framework topology. *Chem Mater* 19:3924–3932. doi:10.1021/cm0705284
72. Williams JJ, Lethbridge ZAD, Clarkson GJ, Ashbrook SE, Evans KE, Walton RI (2009) The bulk material dissolution method with small amines for the synthesis of large crystals of the siliceous zeolites ZSM-22 and ZSM-48. *Microporous Mesoporous Mater* 119:259–266. doi:10.1016/j.micromeso.2008.10.023
73. Kirchner RM, Grosse-Kunstleve RW, Pluth JJ, Wilson ST, Broach RW, Smith JV (2000) Structures of as-synthesized  $\text{AlPO}_4\text{-53(A)}$ , calcined dehydrated  $\text{AlPO}_4\text{-53(B)}$ , and  $\text{AlPO}_4\text{-53(C)}$ , a new phase determined by the FOCUS method. *Microporous Mesoporous Mater* 39:319–332. doi:10.1016/S1387-1811(00)00205-5
74. Amri M, Walton RI (2009) Negative thermal expansion in the aluminum and gallium phosphate zeotypes with CHA and AEI structure types. *Chem Mater* 21:3380–3390. doi:10.1021/cm901140u
75. Attfield MP, Sleight AW (1998) Exceptional negative thermal expansion in  $\text{AlPO}_4\text{-17}$ . *Chem Mater* 10:2013–2019. doi:10.1021/cm9801587
76. Afeworki M, Dorset DL, Kennedy GJ, Strohmaier KG (2006) Synthesis and characterization of a new microporous material. 1. Structure of Aluminophosphate EMM-3. *Chem Mater* 18:1697–1704. doi:10.1021/cm052174r
77. Villaescusa LA, Barrett PA, Cambor MA (1998) Calcination of octadecasil: fluoride removal and symmetry of the pure  $\text{SiO}_2$  host. *Chem Mater* 10:3966–3973. doi:10.1021/cm9804113
78. King RSP, Dann SE, Elsegood MRJ, Kelly PF, Mortimer RJ (2009) The synthesis, full characterisation and utilisation of template-free silica sodalite, a novel polymorph of silica. *Chem Eur J* 15:5441–5443. doi:10.1002/chem.200802551
79. Momma K, Izumi F (2011) VESTA3 for three-dimensional visualization of crystal, volumetric and morphology data. *J Appl Crystallogr* 44:1272–1276. doi:10.1107/S0021889811038970
80. Downs RT, Gibbs GV, Bartelmehs KL, Boisen MB (1992) Variations of bond lengths and volumes of silicate tetrahedra with temperature. *Am Mineral* 77:751–757
81. Woodcock DA, Lightfoot P, Villaescusa LA, Diaz-Cabanás MJ, Cambor MA, Engberg D (1999) Negative thermal expansion in the siliceous zeolites chabazite and ITQ-4: a neutron powder diffraction study. *Chem Mater* 11:2508–2514. doi:10.1021/cm991047q
82. Lightfoot P, Woodcock DA, Maple MJ, Villaescusa LA, Wright PA (2001) The widespread occurrence of negative thermal expansion in zeolites. *J Mater Chem* 11:212–216. doi:10.1039/b002950p
83. Al-Saidi WA, Voora VK, Jordan KD (2012) An assessment of the vdW-TS method for extended systems. *J Chem Theory Comput* 8:1503–1513. doi:10.1021/ct200618b
84. Dobson JF (2014) Beyond pairwise additivity in London dispersion interactions. *Int J Quantum Chem* 114:1157–1161. doi:10.1002/qua.24635
85. Reilly AM, Tkatchenko A (2015) van der Waals dispersion interactions in molecular materials: beyond pairwise additivity. *Chem Sci* 6:3289–3301. doi:10.1039/C5SC00410A
86. Kronik L, Tkatchenko A (2014) Understanding molecular crystals with dispersion-inclusive density functional theory: pairwise corrections and beyond. *Acc Chem Res* 47:3208–3216. doi:10.1021/ar500144s
87. Dovesi R, Orlando R, Civalieri B, Roetti C, Saunders VR, Zicovich-Wilson CM (2005) CRYSTAL: a computational tool for the ab initio study of the electronic properties of crystals. *Z Kristallogr* 220:571–573. doi:10.1524/zkri.220.5.571.65065
88. Combariza AF, Gomez DA, Sastre G (2013) Simulating the properties of small pore silica zeolites using interatomic potentials. *Chem Soc Rev* 42:114–127. doi:10.1039/c2cs35243e
89. Sanders MJ, Leslie M, Catlow CRA (1984) Interatomic potentials for  $\text{SiO}_2$ . *J Chem Soc Chem Commun* 1271–1273. doi:10.1039/c39840001271
90. Cygan RT, Liang J-J, Kalinichev AG (2004) Molecular models of hydroxide, oxyhydroxide, and clay phases and the development of a general force field. *J Phys Chem B* 108:1255–1266. doi:10.1021/jp0363287
91. Piccione PM, Laberty C, Yang S, Cambor MA, Navrotsky A, Davis ME (2000) Thermochemistry of pure-silica zeolites. *J Phys Chem B* 104:10001–10011. doi:10.1021/jp002148a

92. Reilly AM, Cooper RI, Adjiman CS, Bhattacharya S, Boese AD, Brandenburg JG, Bygrave PJ, Bylsma R, Campbell JE, Car R, Case DH, Chadha R, Cole JC, Cosburn K, Cuppen HM, Curtis F, Day GM, DiStasio RA Jr, Dzyabchenko A, van Eijck BP, Elking DM, van den Ende JA, Facelli JC, Ferraro MB, Fusti-Molnar L, Gatsiou C-A, Gee TS, de Gelder R, Ghiringhelli LM, Goto H, Grimme S, Guo R, Hofmann DWM, Hoja J, Hylton RK, Iuzzolino L, Jankiewicz W, de Jong DT, Kendrick J, de Klerk NJJ, Ko H-Y, Kuleshova LN, Li X, Lohani S, Leusen FJJ, Lund AM, Lv J, Ma Y, Marom N, Masunov AE, McCabe P, McMahon DP, Meekes H, Metz MP, Misquitta AJ, Mohamed S, Monserrat B, Needs RJ, Neumann MA, Nyman J, Obata S, Oberhofer H, Oganov AR, Orendt AM, Pagola GI, Pantelides CC, Pickard CJ, Podeszwa R, Price LS, Price SL, Pulido A, Read MG, Reuter K, Schneider E, Schober C, Shields GP, Singh P, Sugden IJ, Szalewicz K, Taylor CR, Tkatchenko A, Tuckerman ME, Vacarro F, Vasileiadis M, Vazquez-Mayagoitia A, Vogt L, Wang Y, Watson RE, de Wijs GA, Yang J, Zhu Q, Groom CR (2016) Report on the sixth blind test of organic crystal structure prediction methods. *Acta Crystallogr Sect B Struct Sci Cryst Eng Mater* 72:439–459. doi:[10.1107/S2052520616007447](https://doi.org/10.1107/S2052520616007447)